

NON-THERMAL X-RAY PROPERTIES OF ROTATION POWERED PULSARS AND THEIR WIND NEBULAE

XIANG-HUA LI^{1,2}, FANG-JUN LU¹ AND ZHUO LI³
ApJ accepted

ABSTRACT

We present a statistical study of the non-thermal X-ray emission of 27 young rotation powered pulsars (RPPs) and 24 pulsar wind nebulae (PWNe) by using the *Chandra* and the *XMM-Newton* observations, which with the high spatial resolutions enable us to spatially resolve pulsars from their surrounding PWNe. We obtain the X-ray luminosities and spectra separately for RPPs and PWNe, and then investigate their distribution and relation to each other as well as the relation with the pulsar rotational parameters. In the pair-correlation analysis we find that: (1) the X-ray (2-10 keV) luminosities of both pulsar and PWN ($L_{X,\text{psr}}$ and $L_{X,\text{pwn}}$) display a strong correlation with pulsar spin down power \dot{E} and characteristic age τ , and the scalings resulting from a simple linear fit to the data are $L_{X,\text{psr}} \propto \dot{E}^{0.92 \pm 0.04}$ and $L_{X,\text{pwn}} \propto \dot{E}^{1.45 \pm 0.08}$ (68% confidence level), respectively, however, both the fits are not statistically acceptable; (2) $L_{X,\text{psr}}$ also shows a possible weak correlation with pulsar period P and period derivative \dot{P} , whereas $L_{X,\text{pwn}}$ manifests a similar weak correlation with \dot{P} only; (3) The PWN photon index Γ_{pwn} is positively correlated with $L_{X,\text{pwn}}$ and $L_{X,\text{pwn}}/\dot{E}$. We also found that the PWN X-ray luminosity is typically 1 to 10 times larger than that from the underlying pulsar, and the PWN photon indices span a range of $1.5 \lesssim \Gamma_{\text{pwn}} \lesssim 2$. The statistic study of PWN spectral properties supports the particle wind model in which the X-ray emitting electrons are accelerated by the termination shock of the wind.

Subject headings: radiation mechanisms: non-thermal - star: neutron - stars: pulsar: general - X-rays: general

1. INTRODUCTION

The rotation-powered pulsars (RPPs) are known as rapidly spinning and strongly magnetized neutron stars that are radiating at the expense of their rotational energy. The X-ray emission of RPPs may contain both thermal and non-thermal components. The thermal emission might be further divided into non-pulsed and pulsed components. The non-pulsed component, originates from the cooling of the neutron star, is from the whole pulsar surface with a characteristic temperature of about 0.1 keV, while the pulsed component comes from hot spots (~ 1.0 keV) on the pulsar surface, which are heated by the bombardment of relativistic particles streaming back to the surface from the pulsar magnetosphere (Kundt & Schaaf 1993, Zavlin et al. 1995, Gil & Krawczyk 1996). The non-thermal pulsar emission is from the pulsar magnetosphere, and it might also contain pulsed (e.g., Cheng & Zhang 1999; Zhang & Harding 2000) and non-pulsed components (e.g., Tennant et al. 2001; Becker et al. 2004). In some cases, a pulsar wind nebula (PWN) is found to surround a RPP. The X-ray emission of the PWN is non-pulsed and often dominates the non-thermal emission of the system.

A lot of efforts have been devoted to the statistical studies of pulsar X-ray emission properties, with particular emphasis on the efficiency of conversion of the pulsar spin down power \dot{E} into X-ray luminosity. By using the *Einstein* data, Seward & Wang (1988) found that $L_X \propto \dot{E}^{1.39}$, where L_X is the 0.2-4.0 keV X-ray luminosity of the pulsar (plus PWN). Becker & Trümper (1997) ob-

tained $L_X \simeq 10^{-3}\dot{E}$ using a sample of 27 pulsars observed by *ROSAT*, where L_X is the total X-ray (0.1-2.4 keV) luminosity of the pulsar plus PWN. However, in these two works, the thermal emission may contribute significantly to the total X-ray luminosity given the adopted soft X-ray band. Saito (1998) analyzed 16 RPPs observed by *ASCA* (2-10 keV) and found $L_X \propto \dot{E}^{3/2}$. Possenti et al. (2002) reported $L_X \propto \dot{E}^{1.34}$ using 39 pulsars observed by *ASCA*, *RXTE*, *BeppoSAX*, *Chandra* and *XMM-Newton*. The X-ray luminosities in Saito (1998) and Possenti et al. (2002) also include the total emission due to the pulsars plus PWNe, given the limited spatial resolutions of *ASCA*, *RXTE*, and *BeppoSAX*. Cheng et al. (2004) divided the total X-ray emission into pulsed and non-pulsed components, and found that the X-ray luminosity of the pulsed one follows $L_{X,\text{pul}} \propto \dot{E}^{1.2}$, which agrees with the model prediction $L_X \propto \dot{E}^{1.15}$ by Cheng & Zhang (1999). For non-pulsed emission, they got $L_{X,\text{npul}} \propto \dot{E}^{1.4}$, where they supposed that the non-pulsed component comes mainly from PWNe and the contribution of non-pulsed component from pulsars is negligible. It is worth noting that the scatter in the relation is large, as pointed out by Possenti et al. (2002), who performed study including the estimates of the observational errors and showing that the linear fit is statistically unacceptable.

All these previous works suffer from the low spatial resolution of the detectors, making it difficult to resolve the emission of the pulsars from that of their surrounding PWNe. It is the purpose of our current work to resolve and to analyze the pulsar and the PWN emission

¹ Laboratory of Particle Astrophysics, Institute of High Energy Physics, CAS, Beijing 100049, China; lixh@ihep.ac.cn; lufj@ihep.ac.cn

² Max-Planck-Institut für Radioastronomie, Auf dem Hügel 69, 53121 Bonn, Germany

³ Physics Faculty, Weizmann Institute of Science, Rehovot 76100, Israel; lizhuo@weizmann.ac.il

separately. Thanks to the high spatial resolution observations performed with *Chandra* and *XMM-Newton*, we have been able to satisfactorily investigate 27 pulsars and 24 PWNe, for which we have determined the non-thermal X-ray fluxes and spectra in the 2-10 keV band. Then we have carried out separated statistic studies of RPPs and PWNe, and tested the consistence of their emission properties with current models. The organization of this paper is as following: the sample and the data processing are presented in section 2; the statistical analyses of the X-ray spectral properties of RPPs and PWNe are given in section 3; we discuss the physical implications of our results in section 4 and summarize our work in section 5.

2. SAMPLE AND DATA PROCESSING

We collect pulsar and PWN samples from the observations by *Chandra* and *XMM-Newton*, which both have high spatial resolutions, i.e., $\sim 1''$ and $\sim 6''$, respectively. We take the *Chandra* data directly from the literatures, and if there are no published results, we analyzed the data in this paper. The *XMM-Newton* data are adapted only if there are no relevant data from *Chandra* for the same source. All the *XMM-Newton* results are taken from literatures. Totally we obtain the X-ray spectra of 27 RPPs and 24 PWNe. In our samples, millisecond pulsars (MSPs) are not included. It is generally believed that MSPs have ever undergone an accretion-driven spin-up phase and they are usually old and regarded as a significantly different class. Similar study on the MSPs is also limited by the rare data available. Therefore we do not analyze MSPs here, although we discuss them when compare our analysis with the previous work including MSPs.

In our samples, there are 15, out of 27, spectra of pulsars obtained from the archived *Chandra* data. We select only the pulsars detected by the Advanced CCD Imaging Spectrometer (ACIS) in the Timed Exposure (TE) Mode, in which a pulsar is able to be resolved spatially from its surrounding PWN. We calibrate the data with CIAO (ver 3.4) and CALDB (ver 3.3.0). We first reprocess the Level 1 data for the correction of the charge transfer inefficiency (CTI) effects, then clean the background and remove the afterglow. Time intervals with anomalous background rates associated with particle flare events are further rejected in the Level 2 data. And then the pulsar positions are obtained by the *celldetect* tool in CIAO. Finally, the spectra are extracted from the Level 2 data and then fit with *XSPEC*. We use both the power-law (PL) and the power-law+blackbody (PL+BB) models to fit the pulsar spectra. If the resulted spectral indices are consistent within errors in both models, then the results from the PL model are used, otherwise those from the PL+BB model are used. In our spectral analysis, we show errors at the 90% confidence level.

Pileup occurs when more than one photon are collected in one pixel within a CCD readout frame, since those photons can only be recorded as a single photon event whose energy is the sum of the collected photons. Therefore pileup may affect the results of spectral analysis. According to section 6.14.2 in the *Chandra* Proposers' Observatory Guide v.7⁴, the effect of pileup can be omitted if the

pileup fraction is $\leq 10\%$. However, pileup does affect the spectral analysis even if the pileup fraction is $\leq 10\%$. For example, since the pileup fraction of PSR J1930+1852 is estimated to be only 6%, its spectral index is reported to be $1.09^{+0.08}_{-0.09}$ without pileup correction (Lu et al. 2002), whileas the spectral index is $1.35^{+0.06}_{-0.10}$ after pileup correction (Camilo et al. 2002). In our spectral analysis, we first estimate the pileup fraction using PIMMS⁵, and then add a pileup model in the spectral fitting of the pulsars if the pileup fraction is higher than 3%. Totally, there are 8 pulsars in which the pileup model is included in the spectral fitting, i.e., PSRs J0205+6449, J0537-6910, B0540-69 (and its PWN), B0833-45 (Vela), J1747-2958, J1846-0258, J1930+1852 and B1951+32.

The absorption column density (N_H) is obtained in several ways. (1) For 6 pulsars (PSRs J0205+6449, J0537-6910, J1747-2958, J1846-0258, J1930+1852 and B1951+32) with bright PWNe, N_H are obtained from the spectral fitting of their PWNe, and then fixed when fitting the spectra of the pulsars. (2) PSRs B0540-69 and J1124-5916 are embedded in SNRs 0540-69.3 and G292.0+1.8, respectively, and their PWN spectra below 2.5 keV are strongly affected by the SNRs. At the same time, constraining N_H with emission above 2.5 keV is difficult because of the small absorption in this high energy range. Therefore their N_H are obtained by fitting the pulsar spectra that the contamination of the SNR emission is negligible, and then N_H are fixed in the spectral fitting of their PWNe. (3) The PWNe associated with PSRs B0355+54, J1617-5055, B1823-13, B1929+10 and J2229+6114 are not bright, and N_H is determined by jointly fitting the spectra of both the pulsar and its PWN. (4) PSRs J0633+1746 and B0833-45 have been studied extensively, and their N_H values used in our spectral fitting are taken from Caraveo et al. (2004) and Pavlov et al. (2001).

The luminosity uncertainty is crucial in our analysis of correlations, and should be considered carefully. Since the X-ray luminosity is given by $L_X = 4\pi d^2 f_X$, where d is the pulsar distance and f_X is the 2-10 keV X-ray flux, the L_X uncertainty should be derived from the uncertainties of both f_X and d . The uncertainty of f_X is derived from those of the normalization and the photon index in the spectral fitting. For the fluxes taken from literatures, their uncertainties are extrapolated from the published ones by the ratios of the fluxes in 2-10 keV to those in the corresponding published energy ranges.

The distances are usually not well constrained, thus the distance uncertainty may dominate the luminosity uncertainty. There are several cases in our samples: (1) the distances of 7 pulsars are derived from the radio dispersion measures, and their errors are conservatively taken to be 40%, as estimated by Cordes & Lazio (2001); (2) the distances of 14 pulsars are obtained via their associated SNRs, and some of them are shown with published distance errors in literatures, while for the others without published errors a conservative error of 50% is taken; (3) PSRs J0537-6910 and B0540-69 are both located in the Large Magellanic Cloud (LMC), whose distance is taken as 50 kpc, and an error of 10 kpc for a conservative esti-

⁴ <http://cxc.harvard.edu/proposer/POG/>

⁵ <http://cxc.harvard.edu/toolkit/pimms.jsp>

mation is adapted (Bradley 2007).

We summarize the properties of all the 27 RPPs and 24 PWNe in Tables 1 and 2, respectively. In Table 2 only 22 PWNe are associated with the RPPs listed in Table 1. The other two pulsars are excluded from Table 1: (1) Camilo et al. (2004) suggested that PSR J1016–5857 is too faint to be resolved from its background PWN in the *Chandra* Observation; (2) Hessels et al. (2004) found that the spectrum of PSR J2021+3651 can be fit by a BB model and is thus dominated by thermal components. On the other hand, 5 out of the 27 RPP samples in Table 1 are not listed in Table 2 for PWNe, because the following 5 pulsars have no PWN reported: B0628–28, B0656+14, B0823+26, B0950+08 and B1055–52 (Ögelman & Tepedelenlioglu 2004, Becker et al. 2004, De Luca et al. 2005).

3. ANALYSES AND RESULTS

The pulsar photon indices are distributed in a range of $1 \lesssim \Gamma_{\text{psr}} \lesssim 3$ (as shown in Fig 1). It should be noted that a significant fraction, about $\sim 15\%$ (4 out of 27), of the sources have soft spectra of $\Gamma_{\text{psr}} > 2$, which may raise problems for current models as discussed later in §4. The photon indices of the PWNe span a narrower range (Fig 1). As discussed below (§4), this is consistent with the pulsar wind model.

We investigate below the correlations between the X-ray emission properties of RPPs and PWNe, and between the emission properties and the pulsar rotational parameters. The rotation parameters include the period P , the period derivatives \dot{P} , and some derived parameters, e.g., the magnetic field $B = 3.3 \times 10^{19} (P\dot{P})^{1/2} \text{G}$, the characteristic age $\tau = P/2\dot{P}$, and the spin down power $\dot{E} = 4\pi^2 I \dot{P}/P^3$, where a typical moment of $I = 10^{45} \text{g cm}^2$ is assumed. We have taken the values of P and \dot{P} from the pulsar catalog by Manchester et al. (2005)⁶.

In order to evaluate the significance level of the correlations of the two parameters concerned, we calculate the widely used Pearson correlation coefficient (r), the Spearman rank correlation coefficient (r_s), and the two-sided significance level (p_s) of the Spearman rank test. The results are listed in Table 3.

In addition to the correlation tests, we also perform a linear fit using the least square method (LSM) to the relevant relations of the parameter pairs. Since the fitting results are usually dominated by a few data points with much smaller observational errors than the others, we also perform a linear fit without the observational errors for comparison. The fitting results are all listed in Table 3, and shown in the relevant figures. In the following we present the results in details.

3.1. Correlations between the RPP emission properties and the pulsar rotational parameters

We study the RPP emission first. Strong correlations appear between the X-ray luminosities of pulsars ($L_{\text{X,psr}}$) and the pulsar rotational parameters (see Table 3 and Figs 2 and 3). First, $L_{\text{X,psr}}$ is negatively correlated with τ and positively correlated with \dot{E} , which are supported by the Spearman tests: $r_s = -0.81$ and $p_s < 0.0001$ between

$L_{\text{X,psr}}$ and τ ; and $r_s = 0.82$ and $p_s < 0.0001$ between $L_{\text{X,psr}}$ and \dot{E} . We also note that there are some hints of the correlation hold for $L_{\text{X,psr}}$ vs P and \dot{P} separately, with the relevant Spearman rank correlation coefficients of -0.66 and 0.69 respectively and both significance levels < 0.001 . The correlations between $L_{\text{X,psr}}$ vs P and \dot{P} will disappear when the sample includes both the MSPs and the normal RPPs, just as shown by Possenti et al. (2002).

Despite the Pearson and Spearman correlation coefficient support the existence of a correlation between $L_{\text{X,psr}}$ and \dot{E} (or τ), a simple linear fit to the logarithm of the data points with the observational errors included does not produce a statistically acceptable model. In fact, it results (here $L_{\text{X,psr}}$ and \dot{E} are in units of erg s^{-1} and τ in years; see also Figs 2 and 3).

$$L_{\text{X,psr}} = 10^{-0.8 \pm 1.3} \dot{E}^{0.92 \pm 0.04} (\chi^2 = 2.6)$$

$$L_{\text{X,psr}} = 10^{38.1 \pm 0.3} \tau^{-1.19 \pm 0.05} (\chi^2 = 4.9)$$

Here and elsewhere in this paper, the uncertainties on the linear fits are reported at 68% confidence level. Previous authors (notably Possenti et al. 2002) also noticed that a large scatter in the plot prevents to obtain an acceptable fit of the data with a simple power law dependence of $L_{\text{X,psr}}$ on \dot{E} . Hence this relation must only be seen as an empirical average trend and not suitable for predicting the luminosity of any specific source.

We have also explored a linear fit which does not account for the uncertainties on the values of $L_{\text{X,psr}}$. It turns out

$$L_{\text{X,psr}}^* = 10^{-4.2 \pm 3.7} \dot{E}^{1.0 \pm 0.1}$$

$$L_{\text{X,psr}}^* = 10^{38.9 \pm 0.9} \tau^{-1.4 \pm 0.2}$$

(see Figs 2 and 3). A comparison between the current $L_{\text{X,psr}}$ versus \dot{E} relation and the previous studies is shown in Fig 2. It can be seen that the relation we obtain above is close to the one between the pulsed X-ray emission and the spin down power in Cheng et al. (2004), which indicates that most of the non-thermal X-ray emission from a pulsar is pulsed.

As already done by Possenti et al. (2002) using a sample including also the MSPs (but not disentangling PWN from RPP emission), we also try to fit L_{X} with $aP^b\dot{P}^c$. This gives the relation

$$L_{\text{X,psr}} = (40 \pm 1) P^{-3.4 \pm 0.3} \dot{P}^{0.77 \pm 0.07} (\chi^2 = 2.5).$$

The nominal result of this (still statistically unacceptable) fit would suggest a preferred dependence of $L_{\text{X,psr}}$ on \dot{E}/P : however we note that, accounting for the uncertainties on the parameters, the simpler dependence on \dot{E} (recovered in the work of Possenti et al. 2002) is also viable.

We also study the pulsar spectral properties, and check if there is any correlation between the pulsar spectral index Γ_{psr} and the pulsar rotational parameters. Inspection of Fig. 4, may indicate the occurrence of a positive correlation of Γ_{psr} with P and τ and of a negative correlation of Γ_{psr} with \dot{P} and \dot{E} . However, a numerical test indicates that all these correlations are too weak (the Spearman coefficients $|r_s|$ are all $\lesssim 0.60$, see Table 3) for drawing any firm conclusion with the available data.

⁶ See <http://www.atnf.csiro.au/research/pulsar/psrcat/>

3.2. Correlations between the PWN emission properties and the pulsar rotational parameters

We study here the correlations between the PWN X-ray luminosity $L_{X,\text{pwn}}$ and the pulsar rotational parameters. As shown in Table 3 and Fig. 5, a weak positive correlation between $L_{X,\text{pwn}}$ and \dot{P} has been detected. Table 3 and Figs 2 and 5 also show that $L_{X,\text{pwn}}$ is strongly correlated with \dot{E} and τ . The linear fits with the observational errors result

$$L_{X,\text{pwn}} = 10^{-19.6 \pm 3.0} \dot{E}^{1.45 \pm 0.08} (\chi^2 = 2.7)$$

$$L_{X,\text{pwn}} = 10^{42.4 \pm 0.5} \tau^{-2.1 \pm 0.1} (\chi^2 = 5.0)$$

Again, $L_{X,\text{pwn}}$ and \dot{E} are in units of erg s^{-1} . Like for the emission from RPPs, the adopted linear model in the logarithm of the data does not provide a statistically acceptable fit.

Trying a linear fit which does not account for the uncertainties on the values of $L_{X,\text{pwn}}$, we obtain

$$L_{X,\text{pwn}}^* = 10^{-14.9 \pm 6.0} \dot{E}^{1.3 \pm 0.2}$$

$$L_{X,\text{pwn}}^* = 10^{40.5 \pm 1.1} \tau^{-1.7 \pm 0.3}$$

We note that the slope of the relation $L_{X,\text{pwn}}^* \propto \dot{E}^{1.3}$ is somewhat different from that of the pulsar, $L_{X,\text{psr}}^* \propto \dot{E}$. The same holds true comparing $L_{X,\text{pwn}} \propto \dot{E}^{1.45}$ with $L_{X,\text{psr}} \propto \dot{E}^{0.92}$. It is worth noting that, as seen in Fig. 2, the scatterings in the relation of $L_{X,\text{psr}}$ versus \dot{E} and that of the PWNe are comparable and both are large.

As seen in Fig 6 and Table 3, there is no evidence for strong correlations between Γ_{pwn} and the pulsar rotational parameters. The Spearman rank test also supports this eye-ball study. However in Figs 1 and 7 we see obvious positive correlations between the photon index Γ_{pwn} and the X-ray luminosity $L_{X,\text{pwn}}$ or the X-ray conversion efficiency $L_{X,\text{pwn}}/\dot{E}$. We will discuss the physical implication in §4.

3.3. Correlations between non-thermal emission properties of RPPs and PWNe

For those samples with both the RPP and the PWN non-thermal X-ray emission measured, we test the correlations between them. As shown in Fig 8, a strong correlation between the X-ray luminosity of RPPs and that of PWNe appears in our samples, while no correlation shown between their photon indices.

The correlation test between two luminosities gives $r_s = 0.91$ and $p_s < 10^{-4}$, and trying a linear fit to the relation leads to $L_{X,\text{pwn}} = 10^{-1.9 \pm 3.2} L_{X,\text{psr}}^{1.1 \pm 0.1}$. Given the strong positive correlations of $L_{X,\text{psr}}$ and $L_{X,\text{pwn}}$ versus \dot{E} separately, a strong correlation between the two luminosities might be naturally expected. However, the slope of the relation between the two luminosities is somewhat different from that expected from the previous two relations, $L_{X,\text{psr}} \propto \dot{E}$ and $L_{X,\text{pwn}} \propto \dot{E}^{1.3}$. This may be because that the samples used are different. For example, those data points with $\dot{E} \lesssim 10^{34} \text{erg s}^{-1}$ are not included for the relation of $L_{X,\text{pwn}}$ versus \dot{E} since no obvious PWNe were detected, and they seem to result in a smaller slope for $L_{X,\text{psr}}$ versus \dot{E} relation (Fig 2). However, it should

be noted that both $L_{X,\text{psr}}$ and $L_{X,\text{pwn}}$ are actually modulated by the source distance. The above correlation might be due to the effect of distance modulation.

In our samples, the X-ray luminosity ratio between PWNe and RPPs, as shown by $f_{X,\text{pwn}}/f_{X,\text{psr}}$ in Fig. 9, varies in the range of $0.1 - 30$, about 2 orders of magnitude, and PWNe are generally brighter than their related RPPs, typically $L_{X,\text{pwn}}/L_{X,\text{psr}} \sim 1 - 10$. Fig. 9 also tells us that a more energetic pulsar does not tend to transfer a bigger fraction of \dot{E} into PWN emission than to the pulsar emission, and vice versa.

Gotthelf (2003) reported a linear relation between Γ_{psr} and Γ_{pwn} for the Crab-like pulsars, but we find no correlation between them in our samples (Fig. 8). We also check the relation using the samples of Gotthelf (2003), and a similar relation appears. These might suggest that the linear relation exists only in the Crab-like pulsars, which are very young.

4. DISCUSSIONS

4.1. Non-thermal X-ray luminosities of RPPs and PWNe

The detected X-ray emission from the RPPs and their PWNe is powered by the pulsar rotation energy. In our sample, the conversion efficiency of \dot{E} to the 2-10 keV X-ray emission varies in the range of $(L_{X,\text{psr}} + L_{X,\text{pwn}})/\dot{E} \sim 10^{-6} - 10^{-1}$, with the mean at $\sim 10^{-3}$, so usually only a small fraction of the spin-down power goes into the non-thermal X-ray emission. The non-thermal X-ray emission in a source is usually dominated by the PWN rather than the pulsar, and on average, $\langle L_{X,\text{pwn}}/L_{X,\text{psr}} \rangle \sim 10$. This implies that the relations of the pulsar X-ray luminosity and the spin-down power obtained in the previous works using the low spatial resolution observations at $> 2 \text{keV}$ might be dominated by the PWN emission.

In this work we can separately analyze the luminosity and the spin-down power relations for the pulsars and their PWNe, thanks to the high spatial resolution of the observations. A strong positive correlation between $L_{X,\text{psr}}$ and \dot{E} is obtained in this paper, similar to the previous results, as shown in Fig 2. We compare our results with the previous work in the following. However, one should keep in mind that there are obvious differences in the analysis processes, i.e., we can separate the RPP and the PWN emission and do not include the MSPs in the sample, while the previous work did not separate the RPPs and the PWNe and included MSPs in the analysis.

The relations for the X-ray luminosity of the RPPs in 2-10 keV band are $L_{X,\text{psr}} \propto \dot{E}^{0.92 \pm 0.04}$ (uncertainties on $L_{X,\text{psr}}$ included) and $L_{X,\text{psr}}^* \propto \dot{E}^{1.0 \pm 0.1}$ (not accounting for the uncertainties on $L_{X,\text{psr}}$), respectively. They are roughly in agreement with the scaling found by Becker & Trümper (1997), who used the X-ray luminosity in the 0.1-2.4 keV band. The $L_X - \dot{E}$ relations obtained by Saito(1998) and Possenti et al. (2002) appear steeper than both our derived relations for RPPs, but they are roughly consistent with both $L_{X,\text{pwn}} \propto \dot{E}^{1.45 \pm 0.08}$ and $L_{X,\text{pwn}}^* \propto \dot{E}^{1.3 \pm 0.2}$ (Fig 2). This may suggest that their relations could also be influenced by the PWN emission due to the lower spatial resolution. The relations $L_{X,\text{pul}} \propto \dot{E}^{1.2 \pm 0.08}$ and $L_{X,\text{npul}} \propto \dot{E}^{1.4 \pm 0.1}$, obtained by Cheng et al. (2004)

with ASCA data, are similar to our results.

We have shown that the weak negative correlation of $L_{X,\text{psr}}$ versus P and the weak positive correlation of $L_{X,\text{psr}}$ versus \dot{P} lead to a strong positive correlation between $L_{X,\text{psr}}$ and \dot{E} in our MSP-excluding RPP samples. On the other hand in the previous work including the MSPs and the normal RPPs, the correlations between the X-ray luminosity (might include the PWN emission) and P or \dot{P} disappear whereas a trend of L_X versus \dot{E} is still there (e.g., Possenti et al 2002). Moreover, the MSP samples alone also obey a similar correlation (Possenti et al. 2002). All these factors together strongly suggest that the X-ray luminosities of RPPs, including the MSPs, are only dependent on their spin-down powers.

Although there is a strong correlation between $L_{X,\text{psr}}$ and \dot{E} , the scattering in this relation is large and the linear fit with the observational errors included usually gives a statistically unacceptable result, as suggested by Possenti et al. (2002). $L_{X,\text{psr}}$ at given \dot{E} may spread over 2-4 orders of magnitude, as seen in Fig 2. The uncertainty in the distance determination and the momenta of inertia are not expected to lead to such a large span, so other intrinsic factors may work, e.g., the viewing angle effect, etc. The scattering in the $L_{X,\text{pwn}} - \dot{E}$ relation is comparably large, which is somewhat strange, since the PWN emission is less influenced by the viewing angles.

4.2. Non-thermal X-ray spectra of the RPPs

There are mainly two scenarios to produce the non-thermal X-rays in the magnetospheres of pulsars. The outer gap scenario (e.g., Cheng et al. 1998; Wang et al. 1998; Cheng & Zhang 1999) produces a downward synchrotron-curvature cascade, where the secondary electrons/positions produce X-rays by synchrotron emission. Another scenario is the polar gap scenario, e.g., Zhang & Harding (2000) proposed the “full polar cap cascade”, where the non-thermal X-rays are produced by resonant inverse Compton (IC) scattering off the thermal X-ray photons. In both scenarios the $L_{X,\text{psr}} \propto \dot{E}$ relation is generally predicted, although the X-ray spectra are not easy to understand.

We note that a significant fraction of pulsars with very soft spectral indices, $\Gamma_{\text{psr}} \sim 2 - 3$, may pose questions on current models. In a cascade, the monoenergetic primary electrons emit monoenergetic curvature photons, which subsequently turn into still monoenergetic pairs in a soft photon bath. The fast energy loss of the secondary pairs in the magnetic field produces synchrotron emission, which have an photon spectrum with a power law index $\Gamma_1 = 1.5$. If the cascade continues the photons produce next-generation pairs and then synchrotron photons with index $\Gamma_2 = 1 + \Gamma_1/2 = 1.75$; furthermore, $\Gamma_3 = 1 + \Gamma_2/2 = 1.875...$ So the indices will never be bigger than 2, in contrast with the soft spectra. Actually this discussion could also work if IC rather than synchrotron emission is involved since the index of synchrotron and IC emission is equal for the same energy distribution of pairs. As for the polar gap scenarios, the synchrotron emission at X-rays is weak because the secondary pairs with small pitch angles produce synchrotron emission well above the cyclotron frequency in the strong pulsar magnetic field,

typically ~ 100 keV. Zhang & Harding (2000) proposed that the X-ray emission is dominated by the low energy tail in the resonant IC emission. However this tail may be hard with index $\Gamma < 2$, as shown in some Monte Carlo simulations (e.g., Fang & Zhang 2006), although the cases might be more complicated when more factors such as the viewing angle are taken into account.

Wang & Zhao (2004) reported the possible negative correlations between Γ_{psr} and $\dot{\Omega}$ and between Γ_{psr} and ζ , where ζ is the generation order parameter characterizing a pulsar under the scheme of cascade processes (Zhao et al. 1989; Lu et al. 1994; Wei et al. 1997). A similar negative correlation between Γ_{psr} and ζ in anomalous X-ray pulsars and softer gamma-ray repeaters had also been reported (Marsden & White 2001; Lu et al. 2003), suggesting that a common mechanism may operate in both normal and anomalous pulsars. These observational results seem in contrast with the predicted positive correlation between Γ_{psr} and ζ by Lu et al. (1994). Here, we also check the relation between Γ_{psr} and the generation order parameter $\zeta_3 = 1 + (0.6 - (11/14)\log P + (2/7)\log \dot{P}_{15})/1.3$ (Eq. 6 of Wang & Zhao 2004) and list the correlation results in Table 3. It turns out that although there may be some hints of such a negative correlation in our sample, the correlation tests do not support it strongly, $r_s = -0.5$. So the current data are not good enough to test the theoretical predictions of Lu et al. (1994).

4.3. X-ray spectra of PWNe

In the standard Kennel & Coroniti (1984ab) model for the Crab nebula, the young Crab pulsar loses its rotational energy predominantly in the form of a highly relativistic particle wind, which encounters with the surrounding medium in a termination shock and become visible by synchrotron emission downstream from the shock. In this context the energy in the relativistic wind is transferred into post shock magnetic field and accelerated particles with energy distribution of $N_e(E_e) \propto E_e^{-p}$. Chevalier (2000) discussed the PWN spectra with emphasis on the cooling of the X-ray emitting electrons, which leads to a steeper index $p+1$ for high energy and fast-cooling electrons, and hence a spectral transition of synchrotron photons from $(p+1)/2$ in the slow-cooling regime to $(p+2)/2$ in the fast-cooling regime at break frequency (ν_c).

The data fit with a single power law model to the indeed broken power law would result in a spectral index always in the range of $(p+1)/2 \leq \Gamma_{\text{pwn}} \leq (p+2)/2$. An electron index value $p \approx 2.2$ is generally obtained in theoretical works on particle acceleration in relativistic collisionless shocks, by both numerical calculations (e.g., Achterberg et al. 2001) and analytic analysis (e.g., Keshet & Waxman 2005), and also inferred from observation in other kinds of astrophysical relativistic shocks, e.g., GRB afterglows (e.g., Freedman & Waxman 2001). Our results show an narrow index range of $1.5 \lesssim \Gamma_{\text{pwn}} \lesssim 2.1$ unless one source with somewhat higher value ~ 2.5 , suggesting an electron index of $p \sim 2.2$. This consistence with particle wind models gives a strong support to the Fermi-shock acceleration in PWNe.

We show that the PWN spectral parameters are not strongly correlated with the pulsar rotational parameters (Fig 6). Gotthelf (2003) reported the correlation between

Γ_{psr} and Γ_{pwn} for nine Crab-like pulsars. Our studies show that such a correlation is probably not a common property for all RPPs. Therefore, the electron spectrum and its evolution in a PWN are not determined by the central pulsar, consistent with wind models where the emission comes from a relativistic shock between wind and environment interaction.

The relation of Γ_{pwn} with PWN luminosity $L_{\text{X,pwn}}$ and the conversion efficiency $L_{\text{X,pwn}}/\dot{E}$ (Figs 1 and 7 and Table 3) could be understood qualitatively in the framework of pulsar wind models taking into account the electron cooling effect on spectral profile (e.g., Chevalier 2000). If pulsar loses most of its rotation energy through particle winds, then higher \dot{E} corresponds to stronger cooling and hence lower spectral break ν_c , which further means a larger index Γ_{pwn} in a fixed observational energy range. In the meantime, a higher \dot{E} corresponds to a larger $L_{\text{X,pwn}}$, no matter ν_c is below or above the observational range, and corresponds to constant X-ray conversion efficiency for fast cooling regime (ν_c below observed range) or larger $L_{\text{X,pwn}}/\dot{E}$ for slow cooling regime (ν_c above observed range). Therefore we have softer PWN spectra (larger Γ_{pwn}) for more luminous PWNe (larger $L_{\text{X,pwn}}$) and higher energy conversion efficiency ($L_{\text{X,pwn}}/\dot{E}$). This consistence supports the wind-shock model for PWNe. In this context, the transition of Γ_{pwn} from high to low values in Fig. 1 suggests that the spectral break ν_c locates at 2-10 keV for $L_{\text{X,pwn}} \sim 10^{33} \text{ ergs s}^{-1}$. This may give constraint to wind model parameters.

5. CONCLUSIONS

In this work, using the available samples of 27 RPPs and 24 PWNe observed by *Chandra* and *XMM-Newton*, we obtain the non-thermal X-ray spectral properties, i.e., luminosities and spectral indices, of RPPs and PWNe separately. We then analyze their distribution and correlation with each other and with pulsar rotational parameters.

- As to the correlations we find: (1) $L_{\text{X,psr}}$ and $L_{\text{X,pwn}}$ display a strong correlation with both \dot{E} and τ ; (2) $L_{\text{X,psr}}$ also shows a possible weaker correlation with P and \dot{P} , whereas $L_{\text{X,pwn}}$ manifests a similar weak correlation with \dot{P} only; (3) Γ_{pwn} is positively correlated with $L_{\text{X,pwn}}$ and the efficiency of conversion of rotational energy loss in X-ray luminosity $L_{\text{X,pwn}}/\dot{E}$.

- Trying to fit the logarithm of the data with a simple linear fit, we find: $L_{\text{X,psr}} = 10^{-0.8 \pm 1.3} \dot{E}^{0.92 \pm 0.04}$ and $L_{\text{X,pwn}} = 10^{-19.6 \pm 3.0} \dot{E}^{1.45 \pm 0.08}$. However, both the fits are statistically unacceptable. Not accounting for the uncertainties on the observed luminosity, the aforementioned relations become $L_{\text{X,psr}}^* = 10^{-4.2 \pm 3.7} \dot{E}^{1.0 \pm 0.1}$ and $L_{\text{X,pwn}}^* = 10^{-14.9 \pm 6.0} \dot{E}^{1.3 \pm 0.2}$, respectively. Since the scatter in the relation for PWN (whose emission should be less affected by viewing angle) is comparably larger than that for RPPs, the scatter in the relation is more probably intrinsic to the sources.
- The PWN X-ray luminosity is typically 1 to 10 times larger than that from the underlying pulsar.
- The pulsar photon index spans a range of $1 \lesssim \Gamma_{\text{psr}} \lesssim 3$. A significant fraction of RPPs with low \dot{E} show soft spectra of $\Gamma_{\text{psr}} > 2$, which seems not consistent with the current models and urges for further investigation of the non-thermal X-ray emission mechanisms of pulsars.
- The PWN spectral properties are consistent with the particle wind model: the photon index range $1.5 \lesssim \Gamma_{\text{pwn}} \lesssim 2$ is consistent with that expected from the shock-accelerated electrons of index $p \sim 2$; the correlations of Γ_{pwn} with $L_{\text{X,pwn}}$ and the conversion efficiency $L_{\text{X,pwn}}/\dot{E}$ are consistent with the wind model; no correlation between Γ_{pwn} and the pulsar rotational parameters also implies that the cooling process is not related to the center pulsars but to the interaction of the pulsar wind with its environment.

ACKNOWLEDGMENTS

We thank the referee for very thorough comments. We are grateful to S. N. Zhang, L. M. Song, J. M. Wang, G. J. Qiao, B. Zhang and H. G. Wang for helpful discussion. We thank Prof. Wielebinski and Dr. Jessner for critically reading the manuscript and giving many valuable suggestions. XHL sincerely thanks Prof. Wielebinski for the financial support during her stay at MPIfR, and thanks J.L. Han for warm hospitality during her stay at NAOC. This work is supported by the National Science Foundation of China through grants 10573017, 10533020 and 10473010.

REFERENCES

- Achterberg, A., Gallant, Y. A., Kirk, J. G., & Guthmann, A. W. 2001, *MNRAS*, 328, 393
- Becker, W., & Trümper, J. 1997, *A&A*, 326, 682
- Becker, W., Weisskopf, M. C., Tennant, A. F., Jessner, A., Dyks, J., Harding, A. K., & Zhang, S. N. 2004, *ApJ*, 615, 908
- Bradley, E. Schaefer 2007, *ArXiv e-prints*, 709, arXiv:0709.4531
- Briskin, W. F., Benson, J. M., Goss, W. M., & Thorsett, S. E. 2002, *ApJ*, 571, 906
- Briskin, W. F., Thorsett, S. E., Golden, A., & Goss, W. M. 2003, *ApJ*, 593, L89
- Camilo, F., Lorimer, D. R., Bhat, N. D. R., Gotthelf, E. V., Halpern, J. P., Wang, Q. D., Lu, F. J., & Mirabal, N. 2002, *ApJL*, 574, L71
- Camilo, F., Gaensler, B. M., Gotthelf, E. V., Halpern, J. P., & Manchester, R. N. 2004, *ApJ*, 616, 1118
- Caraveo, P. A., De Luca, A., Mereghetti, S., Pellizzoni, A., & Bignami, G. F. 2004, *Science*, 305, 376
- Caraveo, P. A., De Luca, A., Mignani, R. P., & Bignami, G. F. 2001, *ApJ*, 561, 930
- Chatterjee, S., Cordes, J. M., Vlemmings, W. H. T., Arzoumanian, Z., Goss, W. M., & Lazio, T. J. W. 2004, *ApJ*, 604, 339
- Cheng, K. S., Gil, J., & Zhang, L. 1998, *ApJ*, 493, L35
- Cheng, K. S., Taam, R. E., & Wang, W. 2004, *ApJ*, 617, 480
- Cheng, K. S., & Zhang, L. 1999, *ApJ*, 515, 337
- Chevalier, R. A. 2000, *ApJ*, 539, L45
- Cordes, J. M., & Lazio, T. J. W. 2002, preprint (astro-ph/0207156)
- Cox, D. P., Shelton, R. L., Maciejewski, W., Smith, R. K., Plewa, T., Pawl, A., & Różyczka, M. 1999, *ApJ*, 524, 179
- De Luca, A., Caraveo, P. A., Mereghetti, S., Negroni, M., & Bignami, G. F. 2005, *ApJ*, 623, 1051
- Faherty, J., Walter, F. M., & Anderson, J. 2007, *Ap&SS*, 308, 225
- Fang, J., & Zhang, L. 2006, *ApJ*, 653, 573
- Freedman, D. L., & Waxman, E. 2001, *ApJ*, 547, 922
- Gaensler, B. M., & Wallace, B. J. 2003, *ApJ*, 594, 326

- Gaensler, B. M., van der Swaluw, E., Camilo, F., Kaspi, V. M., Baganoff, F. K., Yusef-Zadeh, F., & Manchester, R. N. 2004, *ApJ*, 616, 383
- Gil, J., & Krawczyk, A. 1996, *MNRAS*, 280, 143
- Gotthelf, E. V., Halpern, J. P., & Dodson, R. 2002, *ApJ*, 567, L125
- Gotthelf, E. V. 2003, *ApJ*, 591, 361
- Green, D. A., Gull, S. F., Tan, S. M., & Simon, A. J. B. 1988, *MNRAS*, 231, 735
- Hessels, J. W. T., Roberts, M. S. E., Ransom, S. M., Kaspi, V. M., Romani, R. W., Ng, C.-Y., Freire, P. C. C., & Gaensler, B. M. 2004, *ApJ*, 612, 389
- Hui, C. Y., & Becker, W. 2007, *A&A*, 470, 965
- Kargaltsev, O., & Pavlov, G. G. 2007, *ApJ*, 670, 655
- Kaspi, V. M., Gotthelf, E. V., Gaensler, B. M., & Lyutikov, M. 2001, *ApJL*, 562, L163
- Kennel, C. F., & Coroniti, F. V. 1984a, *ApJ*, 283, 694
- Kennel, C. F., & Coroniti, F. V. 1984b, *ApJ*, 283, 710
- Keshet, U., & Waxman, E. 2005, *Physical Review Letters*, 94, 111102
- Koribalski, B., Johnston, S., Weisberg, J. M., & Wilson, W. 1995, *ApJ*, 441, 756
- Kothes, R., Reich, W., & Uyaniker, B. 2006, *ApJ*, 638, 225
- Kramer, M., et al. 2003, *MNRAS*, 342, 1299
- Kundt, W., & Schaaf, R. 1993, *Ap&SS*, 200, 251
- Leahy, D. A., & Tian, W. 2007, *ArXiv e-prints*, 711, arXiv:0711.4107
- Lu, F. J., Wang, Q. D., Aschenbach, B., Durouchoux, P., & Song, L. M. 2002, *ApJL*, 568, L49
- Lu, T., Wei, D.M., & Song, L.M. 1994, *A&A*, 290, 815
- Lu, Y., Wang, W., & Zhao, Y.-H. 2003, *Chinese Journal of Astronomy and Astrophysics*, 3, 543
- Manchester, R. N., Hobbs, G. B., Teoh, A., & Hobbs, M. 2005, *AJ*, 129, 1993
- Marsden, D., & White, N. E. 2001, *ApJ*, 551, L155
- Ögelman, H., & Tepedelenlioğlu, E. 2004, *Advances in Space Research*, 33, 597
- Paron, S. A., Reynoso, E. M., Purcell, C., Dubner, G. M., & Green, A. 2006, *Publications of the Astronomical Society of Australia*, 23, 69
- Pavlov, G. G., Zavlin, V. E., Sanwal, D., Burwitz, V., & Garmire, G. P. 2001, *ApJ*, 552, L129
- Petre, R., Kuntz, K. D., & Shelton, R. L. 2002, *ApJ*, 579, 404
- Possenti, A., Cerutti, R., Colpi, M., & Mereghetti, S. 2002, *A&A*, 387, 993
- Roberts, D. A., Goss, W. M., Kalberla, P. M. W., Herbstmeier, U., & Schwarz, U. J. 1993, *A&A*, 274, 427
- Roberts, M. S. E., Tam, C. R., Kaspi, V. M., Lyutikov, M., Vasisht, G., Pivovarov, M., Gotthelf, E. V., & Kawai, N. 2003, *ApJ*, 588, 992
- Ruiz, M. T., & May, J. 1986, *ApJ*, 309, 667
- Saito, Y. 1998, Ph.D. Thesis, Univ. of Tokyo (S98)
- Seward, F. D., & Wang, Z.-R. 1988, *ApJ*, 332, 199
- Strom, R. G., & Stappers, B. W. 2000, *IAU Colloq. 177: Pulsar Astronomy - 2000 and Beyond*, 202, 509
- Tennant, A. F., et al. 2001, *ApJ*, 554, L173
- Trimble, V., & Woltjer, L. 1971, *ApJ*, 163, L97
- Wang, F. Y.-H., Ruderman, M., Halpern, J. P., & Zhu, T. 1998, *ApJ*, 498, 373
- Wang, W., & Zhao, Y. 2004, *ApJ*, 601, 1038
- Wei, D.M., Song, L.M., & Lu, T. 1997, *A&A*, 323, 98
- Willingale, R., Aschenbach, B., Griffiths, R. G., Sembay, S., Warwick, R. S., Becker, W., Abbey, A. F., & Bonnet-Bidaud, J.-M. 2001, *A&A*, 365, L212
- Zavlin, V. E., Shibano, Y. A., & Pavlov, G. G. 1995, *Astronomy Letters*, 21, 149
- Zhang, B., & Harding, A. K. 2000, *ApJ*, 532, 1150
- Zhao, Y.H., Huang, K.L., Peng, Q.H., Lu, T., & Lu, J.L. 1989, *A&A*, 223, 147

TABLE 1
ROTATIONAL PARAMETERS AND EMISSION PROPERTIES OF 27 PULSARS

PSR Name	P s	\dot{P} s s ⁻¹	N_{H} 10 ²² cm ⁻²	d kpc	Γ_{psr}	f_{X} (2-10keV) ergs s ⁻¹ cm ⁻²	$L_{\text{X,psr}}$ ergs s ⁻¹	Det.	Ref.
J0205+6449	0.066	1.939×10^{-13}	0.442	$3.2^{+1.6}_{-1.6}$	$1.8^{+0.2}_{-0.2}$	$7.4^{+4.7}_{-3.0} \times 10^{-13}$	$9.1^{+24.3}_{-7.8} \times 10^{32}$	C	T, 1
B0355+54	0.156	4.397×10^{-15}	$0.2^{+0.2}_{-0.1}$	$1.0^{+0.2}_{-0.2}$	$1.9^{+0.7}_{-0.5}$	$1.4^{+3.7}_{-1.0} \times 10^{-14}$	$1.8^{+7.7}_{-1.5} \times 10^{30}$	C	T, 2
B0531+21	0.033	4.228×10^{-13}	0.345	$2.0^{+0.5}_{-0.5}$	$1.63^{+0.09}_{-0.09}$	$2.1^{+0.5}_{-0.4} \times 10^{-09}$	$1.0^{+0.9}_{-0.5} \times 10^{36}$	X	3, 4
J0537-6910	0.016	5.178×10^{-14}	0.55	$50.0^{+10.0}_{-10.0}$	$1.8^{+0.2}_{-0.2}$	$1.7^{+0.8}_{-0.5} \times 10^{-12}$	$5.1^{+5.5}_{-2.9} \times 10^{35}$	C	T, 5
B0540-69	0.050	4.791×10^{-13}	$0.43^{+0.18}_{-0.06}$	$50.0^{+10.0}_{-10.0}$	$0.78^{+0.09}_{-0.09}$	$2.9^{+70.5}_{-1.3} \times 10^{-12}$	$8.6^{+307.4}_{-5.6} \times 10^{35}$	C	T, 5
B0628-28	1.244	7.123×10^{-15}	$0.13^{+0.03}_{-0.02}$	$1.4^{+0.6}_{-0.6}$	$2.6^{+0.3}_{-0.3}$	$4.0^{+2.6}_{-1.7} \times 10^{-15}$	$1.0^{+2.3}_{-0.8} \times 10^{30}$	C	6, 7
J0633+1746	0.237	1.097×10^{-14}	0.001	$0.25^{+0.12}_{-0.06}$	$1.8^{+0.2}_{-0.3}$	$2.1^{+1.6}_{-1.0} \times 10^{-13}$	$1.6^{+4.5}_{-1.1} \times 10^{30}$	C	T, 8
B0656+14	0.385	5.500×10^{-14}	$0.043^{+0.002}_{-0.002}$	$0.29^{+0.03}_{-0.03}$	$2.1^{+0.3}_{-0.3}$	$9.6^{+7.6}_{-5.5} \times 10^{-14}$	$9.5^{+11.6}_{-6.2} \times 10^{29}$	X	9, 10
B0823+26	0.531	1.709×10^{-15}	$0.0^{+0.088}_{-0.0}$	$0.3^{+0.1}_{-0.1}$	$2.5^{+0.9}_{-0.5}$	$2.6^{+4.1}_{-2.0} \times 10^{-15}$	$3.6^{+14.8}_{-3.3} \times 10^{28}$	X	11, 7
B0833-45	0.089	1.250×10^{-13}	0.017	$0.29^{+0.08}_{-0.05}$	$1.3^{+0.2}_{-0.1}$	$4.0^{+2.0}_{-1.5} \times 10^{-12}$	$4.2^{+5.8}_{-2.4} \times 10^{31}$	C	T, 12
B0950+08	0.253	2.298×10^{-16}	$0.03^{+0.03}_{-0.02}$	$0.262^{+0.005}_{-0.005}$	$1.9^{+0.1}_{-0.1}$	$5.1^{+1.3}_{-1.0} \times 10^{-14}$	$4.2^{+1.3}_{-0.9} \times 10^{29}$	X	11, 13
B1055-52	0.197	5.833×10^{-15}	$0.027^{+0.002}_{-0.002}$	$0.7^{+0.3}_{-0.3}$	$1.7^{+0.1}_{-0.1}$	$7.8^{+2.8}_{-1.8} \times 10^{-14}$	$4.5^{+8.0}_{-3.4} \times 10^{30}$	X	9, 14
J1124-5916	0.135	7.471×10^{-13}	$0.28^{+0.04}_{-0.04}$	$6.2^{+0.9}_{-0.9}$	$1.62^{+0.10}_{-0.10}$	$6.8^{+2.0}_{-1.5} \times 10^{-13}$	$3.1^{+2.2}_{-1.4} \times 10^{33}$	C	T, 15
J1509-5850	0.089	9.170×10^{-15}	$0.8^{+0.2}_{-0.2}$	$2.6^{+1.0}_{-1.0}$	$1.0^{+0.2}_{-0.3}$	$6.5^{+7.3}_{-3.3} \times 10^{-14}$	$5.3^{+16.1}_{-4.3} \times 10^{31}$	C	16, 7, 14
J1617-5055	0.069	1.351×10^{-13}	$3.3^{+0.3}_{-0.2}$	$3.3^{+1.6}_{-1.6}$	$1.19^{+0.12}_{-0.09}$	$3.4^{+1.3}_{-1.0} \times 10^{-12}$	$4.5^{+9.4}_{-3.6} \times 10^{33}$	C	T, 17
B1706-44	0.102	9.298×10^{-14}	0.55	$2.7^{+0.9}_{-0.9}$	$2.0^{+0.5}_{-0.5}$	$1.1^{+3.0}_{-0.8} \times 10^{-13}$	$9.7^{+54.6}_{-8.4} \times 10^{31}$	C	18, 19
J1747-2958	0.099	6.136×10^{-14}	2.615	$5.0^{+2.5}_{-2.5}$	$1.4^{+0.1}_{-0.1}$	$3.3^{+3.3}_{-2.4} \times 10^{-12}$	$9.9^{+34.9}_{-9.2} \times 10^{33}$	C	T, 20
B1757-24	0.125	1.279×10^{-13}	$3.50^{+1.30}_{-1.10}$	$5.2^{+2.1}_{-2.1}$	$1.6^{+0.6}_{-0.5}$	$6.9^{+9.8}_{-4.4} \times 10^{-13}$	$2.2^{+8.4}_{-1.9} \times 10^{33}$	C	21, 7
J1809-1917	0.083	2.554×10^{-14}	0.72	$3.5^{+1.4}_{-1.4}$	$1.2^{+0.6}_{-0.6}$	$2.5^{+11.4}_{-2.0} \times 10^{-14}$	$3.6^{+36.3}_{-3.4} \times 10^{31}$	C	22, 7
J1811-1925	0.065	4.400×10^{-14}	$2.2^{+0.8}_{-0.6}$	$5.0^{+2.5}_{-2.5}$	$1.0^{+0.4}_{-0.3}$	$2.5^{+2.1}_{-1.3} \times 10^{-12}$	$7.5^{+23.4}_{-6.6} \times 10^{33}$	C	23, 24
B1823-13	0.101	7.506×10^{-14}	$1.0^{+0.6}_{-0.6}$	$3.9^{+1.6}_{-1.6}$	$1.7^{+0.6}_{-0.7}$	$5.4^{+33.3}_{-4.5} \times 10^{-14}$	$9.8^{+130.3}_{-9.2} \times 10^{31}$	C	T, 7
J1846-0258	0.326	7.083×10^{-12}	3.694	$6.0^{+3.0}_{-3.0}$	$1.91^{+0.10}_{-0.10}$	$7.7^{+5.0}_{-3.8} \times 10^{-13}$	$3.3^{+9.0}_{-2.9} \times 10^{33}$	C	T, 25
B1853+01	0.267	2.084×10^{-13}	5.0	$2.6^{+1.3}_{-1.3}$	$1.3^{+0.5}_{-0.5}$	$7.7^{+14.2}_{-5.0} \times 10^{-14}$	$6.2^{+33.6}_{-5.7} \times 10^{31}$	C	26, 27
B1929+10	0.227	1.157×10^{-15}	$0.24^{+0.10}_{-0.09}$	$0.361^{+0.010}_{-0.008}$	$3.0^{+0.4}_{-0.3}$	$5.3^{+5.5}_{-2.7} \times 10^{-14}$	$8.2^{+9.5}_{-4.3} \times 10^{29}$	C	T, 2
J1930+1852	0.137	7.506×10^{-13}	1.6	$5.0^{+2.5}_{-2.5}$	$1.2^{+0.2}_{-0.2}$	$1.8^{+2.1}_{-1.4} \times 10^{-12}$	$5.4^{+21.0}_{-5.1} \times 10^{33}$	C	T, 28
B1951+32	0.040	5.845×10^{-15}	0.299	$2.0^{+1.0}_{-1.0}$	$1.64^{+0.09}_{-0.09}$	$2.0^{+0.8}_{-0.6} \times 10^{-12}$	$9.7^{+20.8}_{-8.1} \times 10^{32}$	C	T, 29
J2229+6114	0.052	7.827×10^{-14}	$0.27^{+0.08}_{-0.07}$	$0.8^{+0.4}_{-0.4}$	$1.05^{+0.10}_{-0.10}$	$3.7^{+1.3}_{-0.7} \times 10^{-13}$	$2.9^{+5.9}_{-2.3} \times 10^{31}$	C	T, 30

Note. — C: *Chandra*, X: *XMM-Newton*

The error bars of f_{X} are derived from the errors in the spectral index and the normalization of spectrum fitting, the error bars of $L_{\text{X,psr}}$ are derived from the errors of both the fluxes and the distances. If more than one papers is listed in Ref. column, the first one is where the spectral properties are from and the other ones are those where the distance is from.

References. — T: This paper; [1] Roberts et al.(1993); [2] Chatterjee et al.(2004); [3] Willingale et al.(2001); [4] Trimble & Woltjer(1971); [5] Bradley(2007); [6] Ögelman & Tepedelenlioğlu(2004); [7] Cordes & Lazio(2002); [8] Faherty et al.(2007); [9] De Luca et al.(2005); [10] Briskin et al.(2003); [11] Becker et al.(2004); [12] Caraveo et al.(2001); [13] Briskin et al.(2002); [14] Kramer et al.(2003); [15] Gaensler & Wallace(2003); [16] Hui & Becker(2007); [17] Paron et al.(2006); [18] Gotthelf et al.(2002); [19] Koribalski et al.(1995); [20] Gaensler et al.(2004); [21] Kaspi et al.(2001); [22] Kargaltsev & Pavlov(2007); [23] Roberts et al.(2003); [24] Green et al.(1988); [25] Leahy & Tian(2007); [26] Petre et al.(2002); [27] Cox et al. (1999); [28] Lu et al.(2002); [29] Strom & Stappers(2000); [30] Kothes et al.(2006).

TABLE 2
EMISSION PROPERTIES OF 24 PWNE

PSR Name	N_{H} 10^{22}cm^{-2}	d kpc	Γ_{pwn}	f_{X} (2-10keV) $\text{ergs s}^{-1} \text{cm}^{-2}$	$L_{\text{X,pwn}}$ ergs s^{-1}	Det.	Ref.
J0205+6449	$0.44^{+0.01}_{-0.01}$	$3.2^{+1.6}_{-1.6}$	$2.07^{+0.02}_{-0.02}$	$5.6^{+0.3}_{-0.3} \times 10^{-12}$	$6.8^{+9.4}_{-5.2} \times 10^{33}$	C	T
B0355+54	$0.2^{+0.2}_{-0.1}$	$1.0^{+0.2}_{-0.2}$	$1.2^{+0.3}_{-0.2}$	$1.4^{+1.2}_{-0.7} \times 10^{-13}$	$1.8^{+3.1}_{-1.2} \times 10^{31}$	C	T
B0531+21	0.345	$2.0^{+0.5}_{-0.5}$	$2.108^{+0.006}_{-0.006}$	$2.1^{+0.1}_{-0.1} \times 10^{-08}$	$1.0^{+0.7}_{-0.5} \times 10^{37}$	X	1
J0537-6910	$0.55^{+0.03}_{-0.03}$	$50.0^{+10.0}_{-10.0}$	$2.43^{+0.06}_{-0.06}$	$2.8^{+0.4}_{-0.4} \times 10^{-12}$	$8.4^{+5.6}_{-3.8} \times 10^{35}$	C	T
B0540-69	0.43	$50.0^{+10.0}_{-10.0}$	$1.96^{+0.08}_{-0.08}$	$5.4^{+1.4}_{-1.1} \times 10^{-12}$	$1.6^{+1.3}_{-0.8} \times 10^{36}$	C	T
J0633+1746	0.001	$0.25^{+0.12}_{-0.06}$	$1.3^{+0.5}_{-0.5}$	$5.1^{+9.0}_{-3.3} \times 10^{-14}$	$3.8^{+19.2}_{-3.1} \times 10^{29}$	C	T
B0833-45	0.017	$0.29^{+0.08}_{-0.05}$	$1.52^{+0.02}_{-0.02}$	$6.2^{+0.4}_{-0.4} \times 10^{-11}$	$6.4^{+4.4}_{-2.3} \times 10^{32}$	C	T
J1016-5857★	$0.3^{+0.7}_{-0.3}$	$3.0^{+0.6}_{-0.6}$	$0.9^{+0.7}_{-0.5}$	$2.3^{+13.4}_{-1.9} \times 10^{-13}$	$2.5^{+21.8}_{-2.2} \times 10^{32}$	C	T, 2
J1124-5916	0.281	$6.2^{+0.9}_{-0.9}$	$1.86^{+0.10}_{-0.10}$	$6.8^{+2.2}_{-1.7} \times 10^{-12}$	$3.1^{+2.3}_{-1.4} \times 10^{34}$	C	T
J1509-5850	$0.8^{+0.9}_{-0.4}$	$2.6^{+1.0}_{-1.0}$	$1.3^{+0.8}_{-0.4}$	$1.5^{+8.0}_{-1.5} \times 10^{-13}$	$1.2^{+13.4}_{-1.2} \times 10^{32}$	C	3
J1617-5055	$3.3^{+0.3}_{-0.2}$	$3.3^{+1.6}_{-1.6}$	$1.1^{+0.3}_{-0.2}$	$3.7^{+2.7}_{-2.3} \times 10^{-13}$	$4.8^{+13.8}_{-4.4} \times 10^{32}$	C	T
B1706-44	$0.6^{+0.2}_{-0.2}$	$2.7^{+0.9}_{-0.9}$	$1.3^{+0.2}_{-0.3}$	$4.0^{+5.7}_{-2.2} \times 10^{-13}$	$3.5^{+11.6}_{-2.8} \times 10^{32}$	C	4
J1747-2958	$2.6^{+0.1}_{-0.1}$	$5.0^{+2.5}_{-2.5}$	$1.93^{+0.10}_{-0.10}$	$4.6^{+1.6}_{-1.2} \times 10^{-12}$	$1.4^{+2.8}_{-1.1} \times 10^{34}$	C	T
B1757-24	3.5	$5.2^{+2.1}_{-2.1}$	$1.0^{+0.6}_{-0.6}$	$1.3^{+3.5}_{-0.9} \times 10^{-13}$	$4.1^{+26.4}_{-3.8} \times 10^{32}$	C	5
J1809-1917	0.72	$3.5^{+1.4}_{-1.4}$	$1.4^{+0.1}_{-0.1}$	$2.3^{+0.8}_{-0.6} \times 10^{-13}$	$3.4^{+5.6}_{-2.5} \times 10^{32}$	C	6
J1811-1925	$2.1^{+0.1}_{-0.1}$	$5.0^{+2.5}_{-2.5}$	$1.7^{+0.2}_{-0.2}$	$3.4^{+1.3}_{-0.8} \times 10^{-12}$	$1.0^{+2.1}_{-0.8} \times 10^{34}$	C	7
B1823-13	$1.0^{+0.6}_{-0.6}$	$3.9^{+1.6}_{-1.6}$	$1.3^{+0.4}_{-0.5}$	$1.4^{+5.3}_{-1.0} \times 10^{-13}$	$2.5^{+21.7}_{-2.3} \times 10^{32}$	C	T
J1846-0258	$3.7^{+0.1}_{-0.1}$	$6.0^{+3.0}_{-3.0}$	$1.89^{+0.05}_{-0.05}$	$2.2^{+0.4}_{-0.3} \times 10^{-11}$	$9.3^{+15.5}_{-7.4} \times 10^{34}$	C	T
B1853+01	5.0	$2.6^{+1.3}_{-1.3}$	$2.2^{+0.2}_{-0.2}$	$2.6^{+1.4}_{-0.9} \times 10^{-13}$	$2.1^{+5.1}_{-1.7} \times 10^{32}$	C	8
B1929+10	$0.24^{+0.10}_{-0.09}$	$0.361^{+0.010}_{-0.008}$	$1.4^{+0.6}_{-0.5}$	$3.8^{+9.6}_{-2.9} \times 10^{-14}$	$5.9^{+16.1}_{-4.6} \times 10^{29}$	C	T
J1930+1852	$1.64^{+0.10}_{-0.09}$	$5.0^{+2.5}_{-2.5}$	$1.89^{+0.10}_{-0.09}$	$5.4^{+1.6}_{-1.3} \times 10^{-12}$	$1.6^{+3.1}_{-1.3} \times 10^{34}$	C	T
B1951+32	$0.30^{+0.01}_{-0.01}$	$2.0^{+1.0}_{-1.0}$	$1.74^{+0.03}_{-0.03}$	$5.1^{+0.4}_{-0.4} \times 10^{-12}$	$2.5^{+3.5}_{-1.9} \times 10^{33}$	C	T
J2021+3651★	$0.8^{+0.2}_{-0.1}$	$8.0^{+4.0}_{-4.0}$	$1.7^{+0.3}_{-0.2}$	$1.1^{+0.5}_{-0.4} \times 10^{-12}$	$8.4^{+19.2}_{-7.2} \times 10^{33}$	C	9
J2229+6114	$0.27^{+0.08}_{-0.07}$	$0.8^{+0.4}_{-0.4}$	$1.0^{+0.1}_{-0.1}$	$4.0^{+2.0}_{-1.3} \times 10^{-13}$	$3.0^{+7.3}_{-2.5} \times 10^{31}$	C	T

Note. — C: *Chandra*, X: *XMM-Newton*

★ PSRs J1016-5857 and J2021+3651 are not listed in Table 1. Their periods are $P = 0.107$ and 0.104 s, respectively, and their period derivatives are $\dot{P} = 8.08 \times 10^{-14}$ and $9.56 \times 10^{-14} \text{s s}^{-1}$, respectively.

The error bars of f_{X} are derived from the errors in the spectral index and the normalization of spectrum fitting. The error bars of $L_{\text{X,pwn}}$ are derived from the errors of both the fluxes and the distances.

References. — T: This paper; [1] Willingale et al.(2001); [2] Ruiz & May(1986); [3] Hui & Becker(2007); [4] Gotthelf et al.(2002); [5] Kaspi et al.(2001); [6] Kargaltsev & Pavlov(2007); [7] Roberts et al.(2003); [8] Petre et al.(2002); [9] Hessels et al.(2004).

TABLE 3
CORRELATION COEFFICIENTS BETWEEN PARAMETERS

y	x	r	r_s	p_s	a_e	b_e	a_{ne}	b_{ne}
$L_{X,psr}$	P	-0.73	-0.66	0.0002	27.1 ± 0.2	-5.2 ± 0.2	28.9 ± 0.7	-3.6 ± 0.7
	\dot{P}	0.70	0.69	0.0001	49.7 ± 0.8	1.29 ± 0.06	51.0 ± 3.9	1.4 ± 0.3
	B	0.41	0.46	0.0165	1.6 ± 1.6	2.5 ± 0.1	10.9 ± 9.4	1.7 ± 0.8
	τ	-0.84	-0.81	$< 10^{-4}$	38.1 ± 0.3	-1.19 ± 0.05	38.9 ± 0.9	-1.4 ± 0.2
	\dot{E}	0.89	0.82	$< 10^{-4}$	-0.8 ± 1.3	0.92 ± 0.04	-4.2 ± 3.7	1.0 ± 0.1
Γ_{psr}	P	0.57	0.60	0.0010	2.03 ± 0.08	0.49 ± 0.08	2.3 ± 0.2	0.7 ± 0.2
	\dot{P}	-0.45	-0.42	0.0274	0.3 ± 0.3	-0.09 ± 0.02	-1.5 ± 1.3	-0.23 ± 0.09
	B	-0.22	-0.22	0.2598	2.5 ± 0.6	-0.08 ± 0.05	4.6 ± 2.6	-0.2 ± 0.2
	τ	0.58	0.44	0.0205	1.0 ± 0.1	0.12 ± 0.02	0.5 ± 0.3	0.26 ± 0.07
	\dot{E}	-0.64	-0.51	0.0067	5.7 ± 0.6	-0.11 ± 0.02	8.5 ± 1.6	-0.19 ± 0.04
	ζ	-0.64	-0.50	0.0081	2.9 ± 0.2	-0.54 ± 0.08	3.8 ± 0.5	-0.9 ± 0.2
	$L_{X,psr}$	-0.55	-0.54	0.0033	5.4 ± 0.5	-0.12 ± 0.02	6.2 ± 1.4	-0.14 ± 0.04
$L_{X,pwn}$	P	-0.54	-0.40	0.0519	29.8 ± 0.3	-3.8 ± 0.3	29.9 ± 1.2	-3.2 ± 1.1
	\dot{P}	0.66	0.61	0.0015	54.3 ± 1.7	1.6 ± 0.1	52.3 ± 4.7	1.5 ± 0.4
	B	0.43	0.52	0.0090	21.2 ± 3.0	1.0 ± 0.2	11.5 ± 9.8	1.7 ± 0.8
	τ	-0.82	-0.76	$< 10^{-4}$	42.4 ± 0.5	-2.1 ± 0.1	40.5 ± 1.1	-1.7 ± 0.3
	\dot{E}	0.86	0.75	$< 10^{-4}$	-19.6 ± 3.0	1.45 ± 0.08	-14.9 ± 6.0	1.3 ± 0.2
	$L_{X,psr}$	0.94	0.91	$< 10^{-4}$	-1.9 ± 3.2	1.08 ± 0.10	-0.3 ± 2.6	1.02 ± 0.08
Γ_{pwn}	P	-0.25	-0.21	0.3216	1.14 ± 0.05	-0.65 ± 0.03	1.2 ± 0.3	-0.4 ± 0.3
	\dot{P}	0.38	0.40	0.0551	4.8 ± 0.2	0.22 ± 0.01	4.1 ± 1.3	0.2 ± 0.1
	B	0.27	0.35	0.0889	-0.2 ± 0.3	0.18 ± 0.03	-1.5 ± 2.4	0.2 ± 0.2
	τ	-0.45	-0.45	0.0279	2.94 ± 0.04	-0.27 ± 0.01	2.5 ± 0.4	-0.22 ± 0.09
	\dot{E}	0.45	0.43	0.0367	-5.7 ± 0.3	0.203 ± 0.008	-4.3 ± 2.4	0.16 ± 0.07
	Γ_{psr}	-0.01	0.04	0.8554	0.2 ± 0.3	1.1 ± 0.2	1.6 ± 0.3	-0.01 ± 0.20
	$L_{X,pwn}$	0.70	0.70	0.0001	-4.9 ± 0.7	0.20 ± 0.02	-3.8 ± 1.2	0.16 ± 0.04
	$L_{X,pwn}/\dot{E}$	0.73	0.75	$< 10^{-4}$	3.2 ± 0.2	0.46 ± 0.08	2.6 ± 0.2	0.31 ± 0.06
$f_{X,pwn}/f_{X,psr}$	\dot{E}	0.13	0.15	0.4917	-2.3 ± 5.7	0.07 ± 0.15	-20.6 ± 43.4	0.7 ± 1.2

Note. — r is Pearson correlation coefficient, while r_s and p_s are Spearman rank correlation coefficient and significance level, respectively. Coefficients a_e and b_e (a_{ne} and b_{ne}) are obtained in the linear fitting with (without) observational errors.

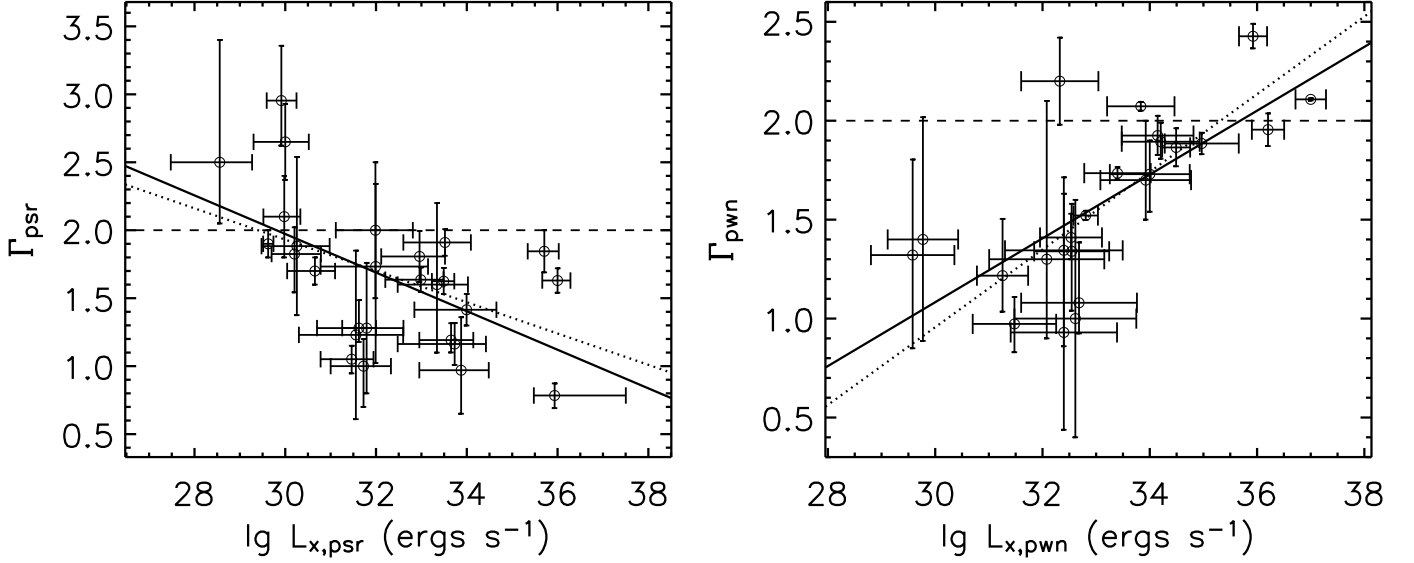


FIG. 1.— The relations between the non-thermal X-ray luminosity in 2-10 keV and the photon index for RPPs (left panel) and PWNe (right panel). The solid lines are the best LSM fit without observational errors taken into account, while the dotted line with observational errors. The dashed lines mark the cases of $\Gamma=2$ for comparisons.

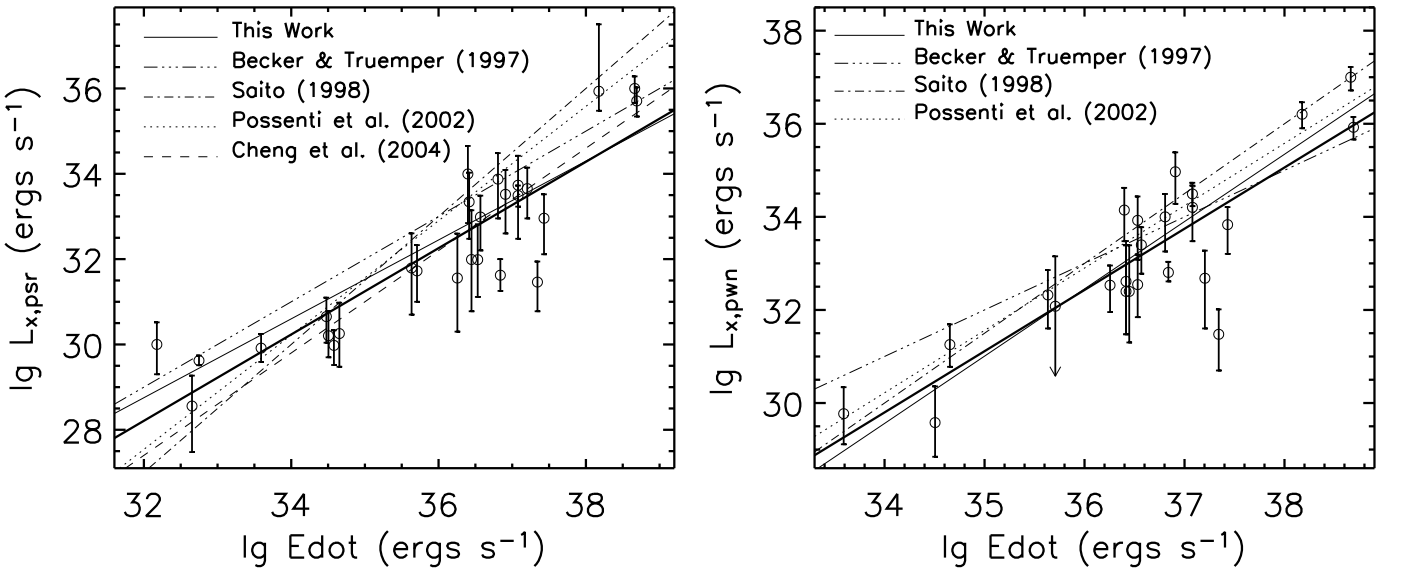


FIG. 2.— Left: The non-thermal X-ray luminosities ($L_{\text{x,psr}}$) in 2-10 keV from the *Chandra* and *XMM-Newton* observations vs. spin-down power \dot{E} of 27 pulsars. Right: The non-thermal X-ray luminosity ($L_{\text{x,pwn}}$) in 2-10 keV from the *Chandra* and *XMM-Newton* observations vs. spin-down power \dot{E} of 24 PWNe. The bold solid line is the best fit to the data by LSM without observational errors included, while the thin solid line is the fit with observational errors. For comparison the resulted relations in previous works are also marked: the dash-dot-dot-dot line corresponds to results of Becker & Trümper (1997); the dash-dot line to Saito (1998); the short dash line to Possenti et al. (2002); and long dash line to Cheng et al. (2004).

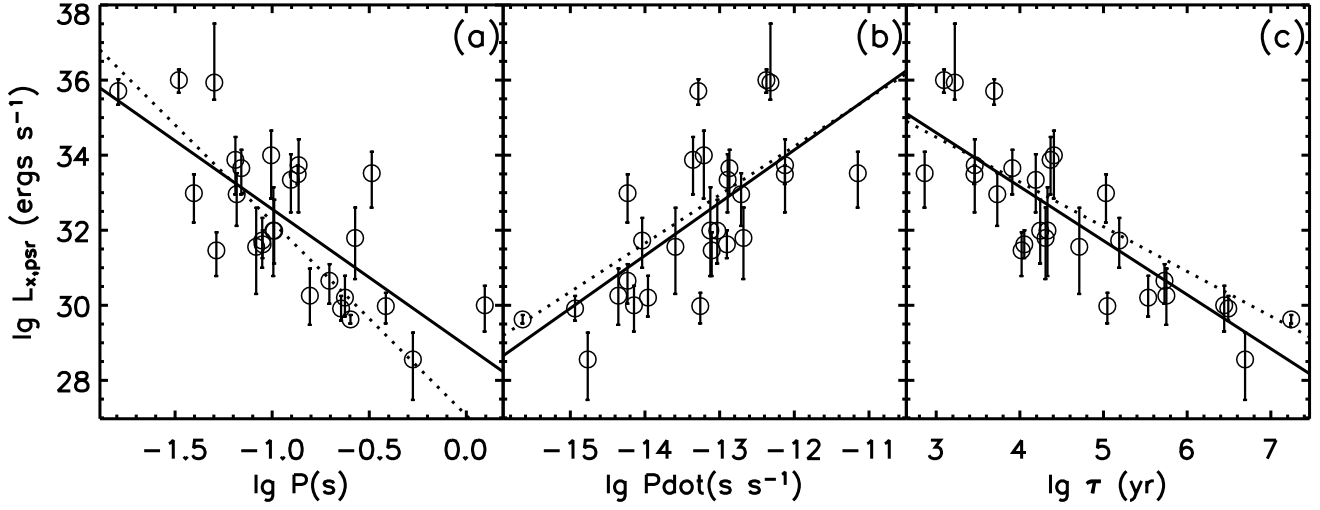


FIG. 3.— Relations of $L_{X,\text{psr}}$ vs. P , \dot{P} and τ . The solid lines are the best LSM fit without observational errors considered while the dotted lines are with errors. The fitting results are also listed in Table 3.

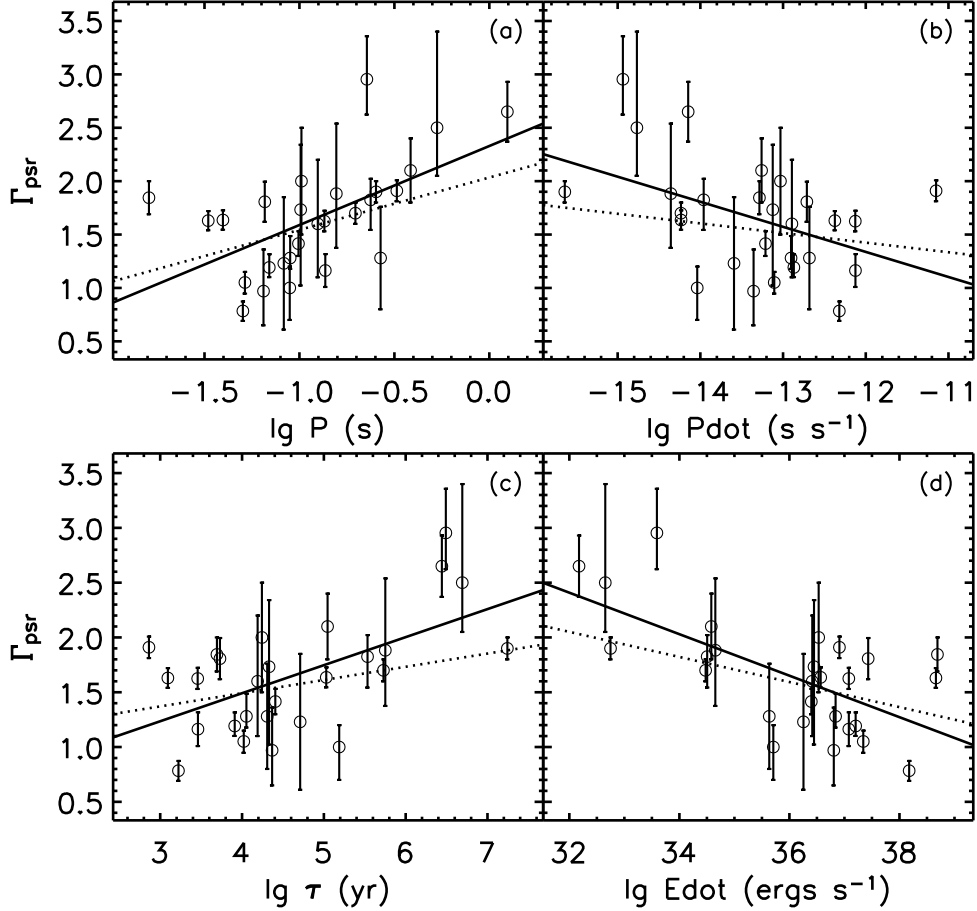


FIG. 4.— Relations of Γ_{psr} vs. P , \dot{P} , τ and \dot{E} . The solid lines are the best LSM fit without observational errors considered while the dotted lines are with errors. The fitting results are also listed in Table 3.

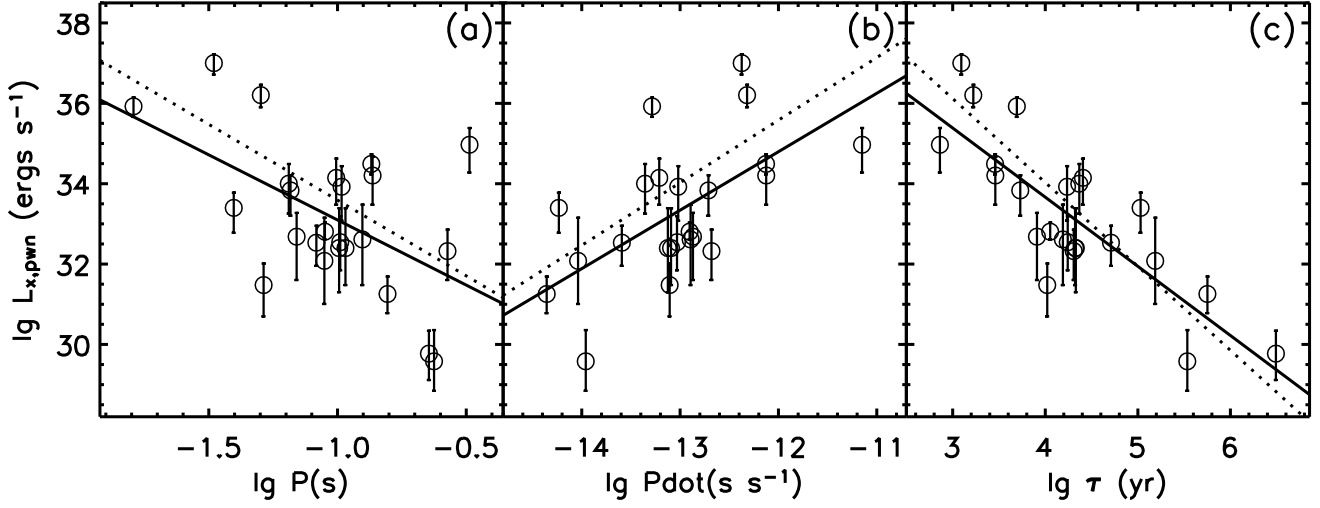


FIG. 5.— Relations of $L_{X,pwn}$ vs. P , \dot{P} and τ . The solid lines are the best LSM fit without observational errors considered while the dotted lines are with errors. The fitting results are also listed in Table 3.

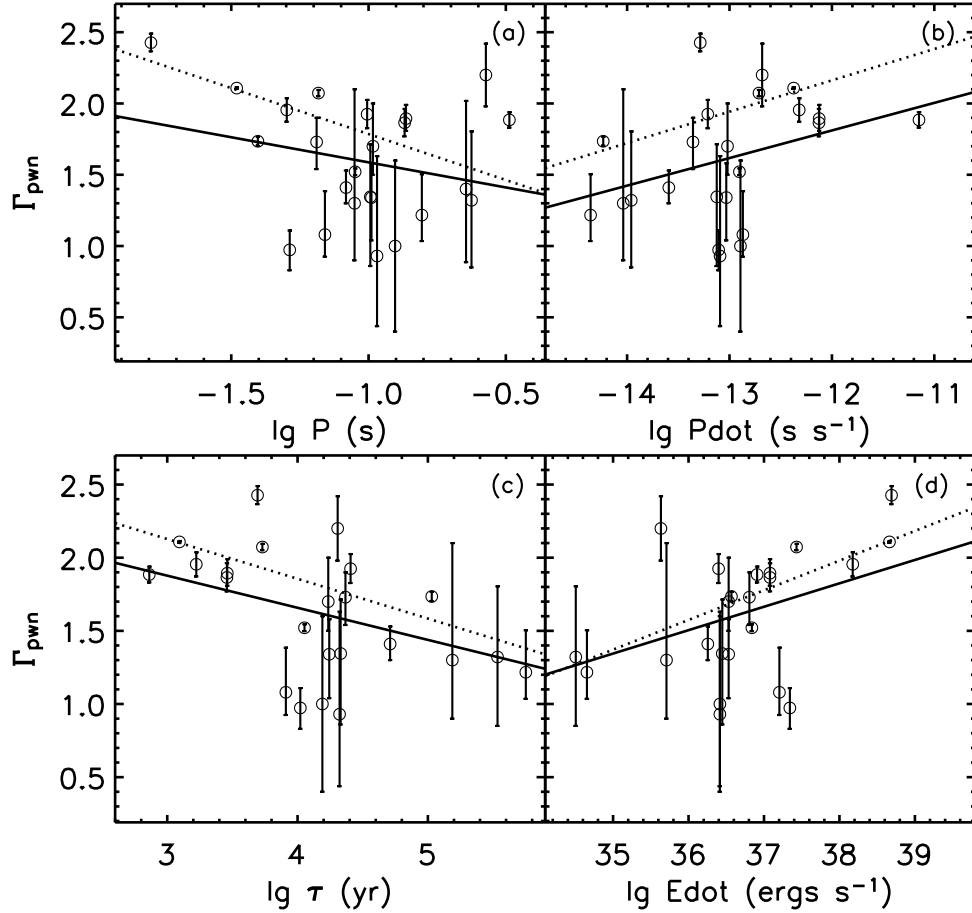


FIG. 6.— Relations of Γ_{pwn} vs. P , \dot{P} , τ and \dot{E} . The solid lines are the best LSM fit with observational errors considered while the dotted lines are without errors. The fitting results are also listed in Table 3.

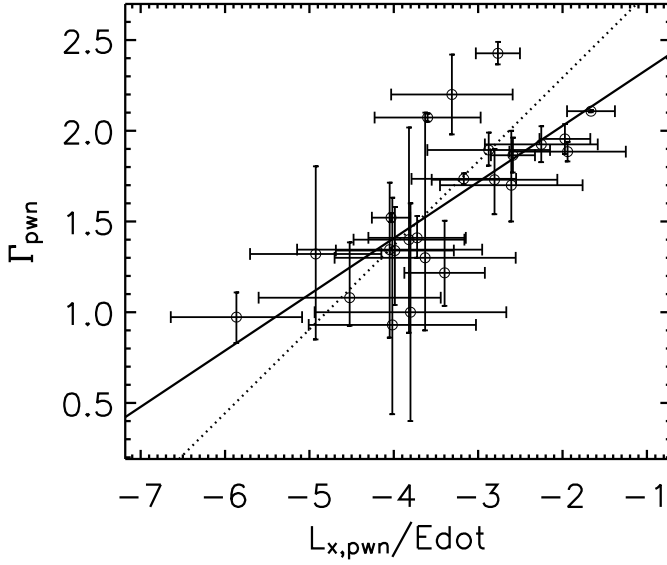


FIG. 7.— The relation between Γ_{pwn} and $L_{\text{X,pwn}}/\dot{E}$. The solid line is the best LSM fit without observational errors considered while the dotted line is with errors. The fitting results are also listed in Table 3.

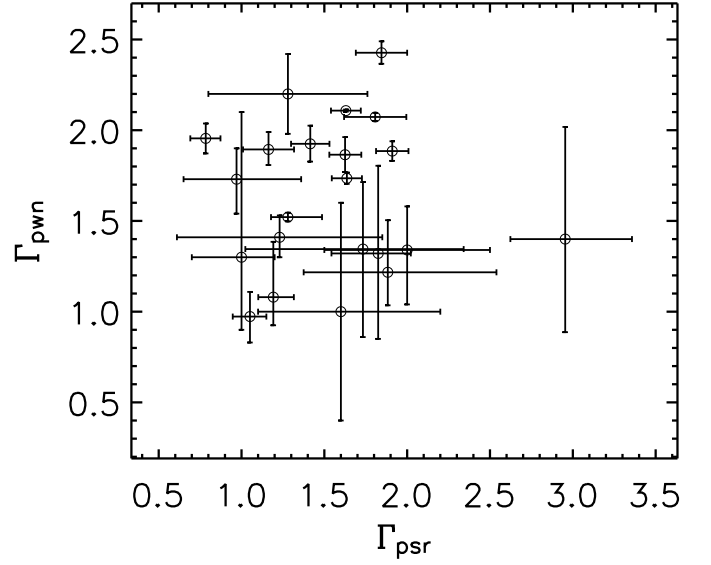
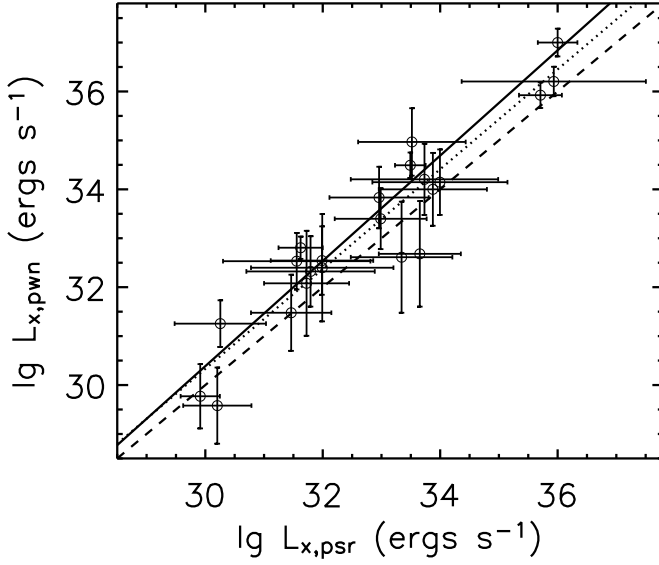


FIG. 8.— Left: the relation of $L_{\text{X,psr}}$ vs. $L_{\text{X,pwn}}$. The solid lines are the best LSM fit with the observational errors considered while the dotted lines are without errors. The fitting results are also listed in Table 3. The dash line marking the case of $L_{\text{X,psr}} = L_{\text{X,pwn}}$ is for comparison. Right: the relation of Γ_{psr} vs. Γ_{pwn} .

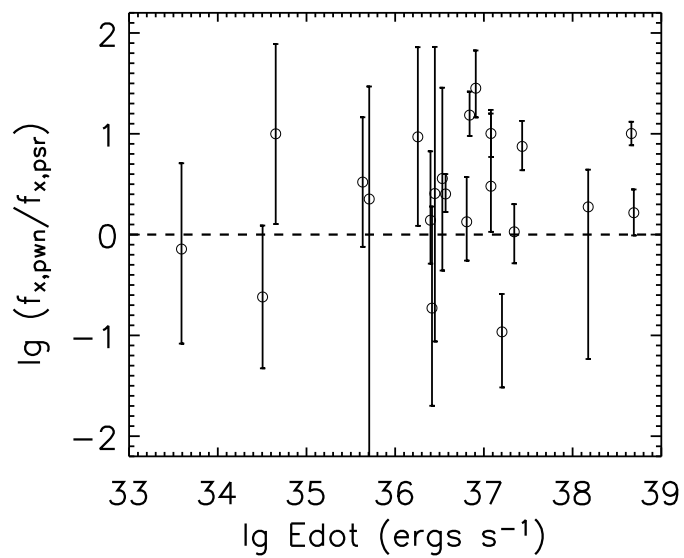


FIG. 9.— The relation of $f_{X,pwn}/f_{X,psr}$ vs \dot{E}_x . The dash line indicates $f_{X,pwn} = f_{X,psr}$.